Heliyon 9 (2023) e14751

Contents lists available at ScienceDirect

Heliyon

journal homepage: www.cell.com/heliyon

Research article

Combined effect of seawater and load on methacrylate adhesive

Francisco J. Rodríguez-Dopico [a,*], R.J.C. Carbas [b], Catarina S.P. Borges [b], J. Tarrío-Saavedra [c], L.F.M. da Silva [d], A.Álvarez García [a]

[a] Universidade da Coruña, Campus Industrial de Ferrol, Departamento Ingeniería Naval e Industrial, Escola Politécnica de Enxeñaría de Ferrol, Grupo de Propiedades Térmicas y Reológicas de Materiales, Ferrol, 15403, A Coruña, Spain
[b] Institute of Science and Innovation in Mechanical and Industrial Engineering (INEGI), Porto, Portugal
[c] Grupo MODES, CITIC, Departamento de Matemáticas, Escola Politécnica de Enxeñaría de Ferrol, Universidade da Coruña, Ferrol, Spain
[d] Department of Mechanical Engineering, University of Porto, Porto, Portugal

ARTICLE INFO

Keywords:
Adhesive
Diffusion
Aging
Seawater
Shipbuilding
Load

ABSTRACT

Although the shipbuilding industry is constantly demanding new advanced joining solutions, adhesive technology is not as developed in the marine as compared to other industries. The main reason is the lack of specific knowledge that guarantees the durability of the bonded joints in optimal conditions during the life cycle of a ship. This work simulates in the laboratory a marine-like environment by immersing an adhesive in seawater and subjecting it to constant loading. The objective is to characterize the seawater absorption behavior and its consequences on the mechanical, thermal, and chemical properties of the adhesive after this aging process. Seawater ingress was determined through gravimetric tests at several load conditions of the tensile strength of the adhesive. Besides, absorption process was studied using Fick's Law, determining the diffusion coefficients. The thermal behavior was monitored with differential scanning calorimetry (DSC) and the chemical degradation was analyzed using Fourier transform infrared spectroscopy (FTIR). Also, the mechanical properties were determined by tensile tests. The surface of the adhesive (dried) was studied by Scanning Electron Microscopy (SEM) technique and the porosity was measured by physisorption with a high-performance adsorption analyzer. A numerical simulation was developed using Darcy's Law combined with continuity equation. The results show that application of loads and immersion in seawater until full saturation of seawater improve the mechanical properties of the adhesive, but it affects negatively to the glass transition temperature. This should be considered when designing adhesive bonding joints on ships.

1. Introduction

Adhesive bonding presents interesting advantages when compared to traditional joining techniques, such as welding, mechanical fastening, and riveting, which are widely used in the shipbuilding industry: It is a lightweight and corrosion-resistant way of joining materials; it provides lower stress concentration along the joint and it can be used for bonding different materials, such as steel and composites; it is easier and faster to apply during construction process (especially when working in confined-spaces) and it is also advantageous from the point of view of managing the health and safety of shipyard welders, because not only are hot work and fire risks are avoided in adhesive application during construction, but also the exposure to metal fumes and hazardous air pollutants

* Corresponding author.
E-mail address: f.j.rodriguez@udc.es (F.J. Rodríguez-Dopico).

https://doi.org/10.1016/j.heliyon.2023.e14751
Received 19 November 2022; Received in revised form 9 March 2023; Accepted 16 March 2023
Available online 22 March 2023

produced by welding processes that might produce several diseases [1–3]. The implementation of adhesion technology in the shipyard's production processes would produce an increase in productivity, simplify design constraints and lead to a significant decrease in ship weight [4]. The latter is directly related to the energy efficiency and reduction of carbon emissions into the atmosphere, improving the environmental footprint. Marine global shipping emitted about 3.1% of global CO_2 emissions in 2012. It is expected to increase these emissions levels by 50–250% in 2050. So, the impact and transcendence of implementing this type of solutions among other technologies will be global [5–7].

The naval sector demands specific knowledge about the long-term behavior and durability of adhesive joints in the marine environment [8]. The whole shipbuilding industry (shipyards, universities, research centers, classification societies, manufacturers) is cooperating in the search for new technological solutions to generate an understanding of the adhesive bonding for its implementation and certification in safe conditions in the ship [9–14].

To date, several studies have investigated the environmental effects on adhesive bonding in the marine field. E. Lertora et al. did not find significant variations after immersion in saline solution in the mechanical resistance of a methacrylate adhesive itself, but not for the joints, as the corrosion of metallic surfaces noticeably reduces the resistance at the interface, causing breakages [15]. Sánchez-Amaya et al. stated that static and fatigue mechanical properties of bonded coated steel joints are improved with aging in seawater during the first month of exposure [16]. Arnaud et al., proposed a constitutive model depending on the moisture concentration to describe the 3D behavior of an adhesive in an assembly exposed to a marine environment [17]. Hayashibara et al., after studying the degradation process in different conditions, determined a design temperature of at least 70 °C for adhesive bonding on exposed decks of ocean-going vessels [18]. Momber et al. investigated the performance of adhesive joints between stainless steel brackets and coated steel substrates, concluding that there was a high mechanical stability, but avoiding the ingress of moisture in a thoroughly sealed joint [19]. Alia et al. studied the degradation of structural adhesives of polyurethane and vinylester in seawater for different periods of time, concluding there is an irreversible damage in the polymer properties in a determined time that negatively affect their mechanical properties [20].

The water absorbed by an adhesive affects its physical and mechanical properties producing reversible (swelling, plasticization) or permanent changes (causing crack, craze, or hydrolysis). There is also a coupling between mechanical loading and water diffusion, as mechanical loads have been seen to accelerate water absorption, and water affects the stresses produced in a joint [21]. Temperature must be considered as an important degradation factor. The T_g is defined as "the temperature at which the transition between the glassy and rubbery state of amorphous solids occurs" and it is considered the most relevant thermal property of a cured adhesive. Also it is important to highlight that water uptake performance of the polymer depends on the T_g [22].

Water diffusion is usually studied with Fick's Law [23], which generally provides a good explanation to this phenomenon. Fickian behavior is presented if the diffusion rate is much quicker than the relaxation rate, and non-Fickian one occurs when the relaxation rate influences the water uptake [24–26].

Furthermore, previous studies focused on molecular diffusion on a porous media were performed in recent years. Regarding the use of molecular dynamics simulations, Chen et al. [27] studied the chloride transport under electric field in C–S–H nanopores of cement-based materials, concluding that, with greater intensity, chloride ions are moved towards the center of the pore and the diffusion coefficient is increased by two orders of magnitude. Moreover, Tartakovsky et al. [28] presented a pore-scale representation of diffusion by introducing models of molecular diffusion in the presence of geometric constraints imposed by the solid matrix of a porous medium, including also a discussion on phenomenological Darcy-scale descriptors of pore-scale diffusion. In addition, Starov et al. [29] found a good agreement between the experimental data and a theorical method that deduce a dependence of the effective diffusion coefficient in porous media on the porosity in composite materials.

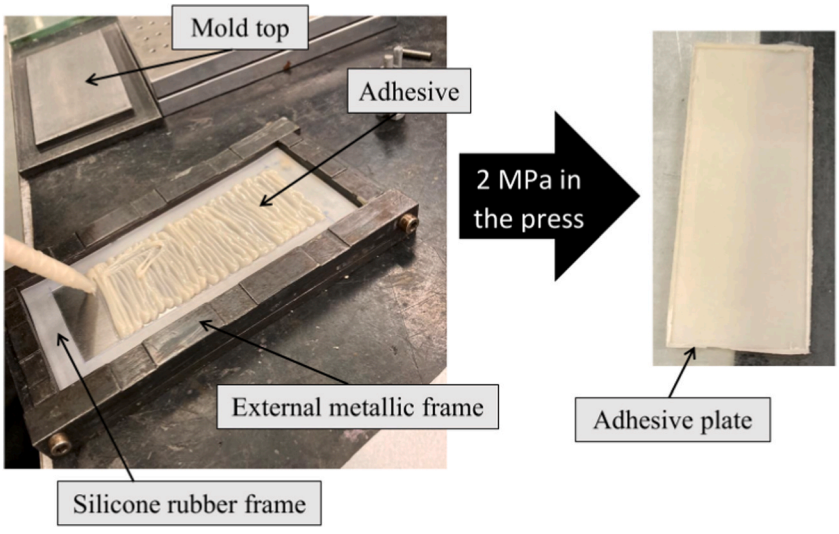

Fig. 1. Mold used to manufacture adhesive plates.

Concluding, the purpose of the present investigation is to analyze the effect of the combined influence of three different constant load conditions and seawater diffusion factors on the mechanical, thermal, and chemical properties of a methyl methacrylate adhesive immersed in seawater.

2. Materials and methods

2.1. Adhesive

A methyl methacrylate-based adhesive (Acralock SA1-05A) has been chosen to conduct this work, since its application for bonding metal substrates is recommended. It is a two-part adhesive which is formulated to be primer except on most metal surfaces. Mixed at room temperature with 1:1 ratio, it has a handling time of 5–8 min and 15–20 min of fixture time. The operating temperature of the adhesive is between −40 and 82 °C. Adhesives, technical and safety data sheets were supplied by the manufacturer, Engineered Bonding Solutions, LLC, Florida, United States.

2.2. Specimen manufacturing

The methyl methacrylate-based adhesive specimens are composed of, was as said, a two-component system. The mixing and application were carried out with a manual gun equipped with a nozzle. The resulting blend was significantly viscous. Therefore, the method chosen for manufacturing was insertion into a mold, lined with a 1 mm thick silicone frame as shown in Fig. 1, applying pressure between the mold plates as described in the French Standard NF T 76–142 [30] and da Silva et al. [31]. This technique has been used in previous studies [16,32,33] and is especially appropriate for producing plates without bubbles since the silicone frame, along with ensuring the correct thickness of the adhesive, promotes hydrostatic pressure. So, the manufactured plates of adhesive were cured at room temperature in a mold with a silicone rubber frame under high pressure (2 MPa). Previously, a slightly higher amount of adhesive than the corresponding volume to the internal part of the silicone rubber frame was placed in the center part of the mold, which was introduced in the press applying pressure for the curing time stated by the manufacturer. After that, plates were cut according to the dimensions required for each test.

2.3. Experimental design

Adhesive samples were immersed in seawater under three different load conditions: 0%, 5% and 15% of the tensile strength. An experimental setup was designed specifically for this study (Fig. 2): A tempered glass container full of seawater in which a stainless-

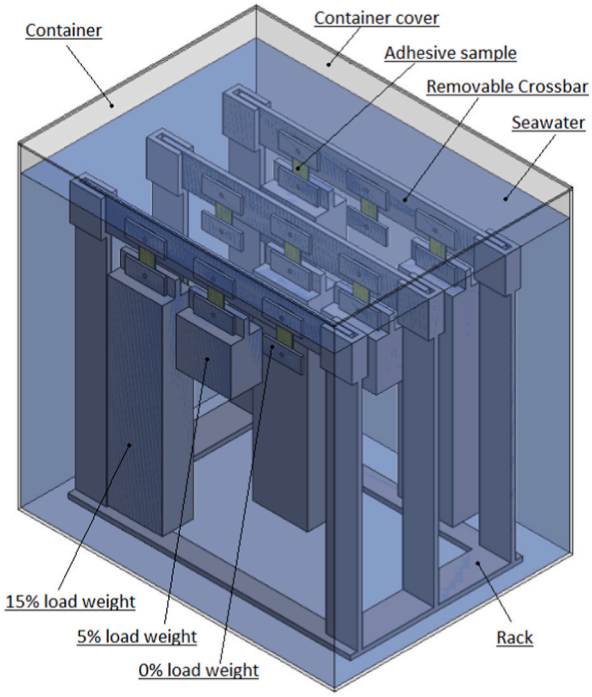

Fig. 2. Experimental setup: Rack inside a tempered glass container (400 mm width × 400 mm height × 300 mm depth) holding specimens with different loads applied. Dimensions of each 15% load condition weight are 70 mm width × 135 mm height × 40 mm depth. For 5% load condition weights, dimensions are 70 mm width × 43 mm height × 40 mm depth.

steel rack is introduced, holding the adhesive samples and lead weights. The load range chosen is given mainly by two circumstances. Firstly, physical limitations, such as the dimensional limit of the climate chamber and the size of the weights. Secondly, an upper limit of 15% of the tensile strength is sufficient and higher than the load that the adhesive would undergo in its application in the ship.

There are three rows, equivalent to each other, where three loading conditions are studied in each one. The design assures a constant separation between samples and the container. The upper crossbars are removable, facilitating the introduction and extraction of samples to perform the gravimetric analysis during the aging process (Fig. 3).

The constant temperature of 48 °C of seawater during the aging process was controlled by placing the container in a climatic chamber (Memmert GmbH, Büchenbach, Germany) (Fig. 4). Gravimetric weighing was taken in the shortest possible time, at 24-h intervals, ensuring that both the seawater and the specimens were stabilized at this temperature inside the climatic chamber. The present study is focused on marine bonding applications indoors, where average maximum temperatures during winter and summer in the interior compartments of a ship (machinery room, laundry, kitchen, cabins) have been considered to set the chosen study temperature.

The determination of the mass of each block, according to different load levels chosen, was achieved from the geometry of the specimens and the strength given by the manufacturer. Considering that the dimensions of each sample are 1 mm thickness, 20 mm width, 60 mm length and according to manufacturer's datasheet, the tensile strength is 20.7 MPa, each mass was calculated following equation (1):

$$Mass = wh\frac{\%\sigma_{adh}}{g} \tag{1}$$

where % σ_{adh} is the percentage per condition studied (0%, 5%, 15%) of the total value of the tensile strength in MPa, w is the width in mm, h is the thickness in mm of the specimen, g is the gravity in m•s^{-2}, and the *mass* is the weight in Kg.

The material chosen to manufacture each block was lead (Pb), due to its high specific weight, allowing the blocks to have the intended mass, reaching the desired percentage of the tensile strength with manageable dimensions. Therefore, the mass correspondent to the application of constant loads of 5% and 15% of the tensile strength (20.7 MPa) were defined. The weights of the fastening components used (nuts, washers, pins, screws, plates) have been considered for each load level and the conclusion is that they can be considered negligible in terms of determination of each mass. Results are presented in Table 1.

Tensile strength was also calculated from tensile tests on bulk specimens and compared with the value given by manufacturer. There is an error of 6.3% between manufacturer's tensile strength results of 20.7 ± 0.1 MPa and the average tensile strength obtained experimentally of 19.4 ± 0.1 MPa. It can be inferred from the results that the experimental values obtained agree with those provided by the manufacturer and therefore validate the calculations previously made according to equation (1).

Fig. 3. Second rack outside the container, used to hold the upper crossbars with samples during gravimetric analysis.

Fig. 4. Container with specimens in the climatic chamber.

Table 1
Determination of the mass of blocks for different constant loads, considering the fastening elements.

Load level	Mass (kg) (calculated)	Mass (kg) fastening elements
0%	0.00	0.06
5%	2.07	0.06
15%	6.21	0.06

2.4. Gravimetric analysis

Gravimetric test specimens were shaped in 1 mm thick plates of 60 mm length, 20 mm width, and kept in a sealed container with silica gel beads until complete drying was assured (difference between successive weighing values less than 0.1 mg). After this, the surface of the specimens was smoothed, eliminating possible contaminants, and minimizing the effect of surface roughness on the water absorption behavior. Fine sandpaper of grade FEPA P#4000 was used. Once this process was completed, each specimen was weighed to determine its mass prior to immersion in seawater.

The behavior of the adhesive under different constant load conditions was studied for each specimen through aging with different weights applied: 0%, 5% and 15% load of the tensile strength. Measurements were always performed using a caliper to assure the same area of water absorption. Complete immersion of all specimens along their entire length, not only in the absorption zone, was ensured. Each specimen was weighed periodically, removing it from the container and wiping off the surface with a paper towel before each weighing to eliminate water that might be on the surface of the specimens. Data was recorded until full saturation was reached. All weight measurements were performed using a microbalance with an accuracy of 0.1 mg (KernToledo, Balingen, Germany). The water uptake of each specimen, for each measurement, was given by equation (2):

$$M_t = \frac{m_t - m_0}{m_0} \times 100(\%) \tag{2}$$

where m_t is the mass of the specimen at the current time measurement and m_0 is the initial mass of the specimen. The saturation of the specimens was considered complete when the water uptake value was stable because the material was unable to absorb more water.

2.4.1. Differential scanning calorimetry (DSC)

Disks of 6 mm diameter for differential scanning calorimetry (DSC) were obtained from the unaged (dried) and aged adhesive specimens of 1 mm thick for the conditions analyzed. Thermal behavior of the adhesive was studied prior and after the aging process at different constant loads using a DSC 214 Polyma DSC21400A-0655-L machine (NETZSCH-Gerätebau GmbH, Selb, Germany). For the specimen prior aging, temperature changed between 20 and 150 °C; then, the samples were cooled from 150 to 20 °C and finally heated from 20 to 150 °C, which was the range considered for the analysis. The heating and cooling were performed at 10 °C/min in a N_2 atmosphere. For the aged specimens, same procedure was adopted, but using a different temperature range: 20–200 °C.

2.5. Fourier transform infrared spectroscopy (FTIR)

Disks of 6 mm diameter for Fourier-transform infrared (FTIR) were obtained from the unaged (dried) and aged adhesive specimens of 1 mm thick for the conditions analyzed. The FTIR analysis was carried out using a PerkinElmer Spectrum Two machine (Waltham, MA, USA). Wave lengths of 4000–500 cm^{-1} were used at a scanning velocity of 0.2 cm^{-1}. Tests were performed with a $LiTaO_3$ detector

(15,700–370 cm^{-1}) and a KBr window. The spectra were obtained in attenuated total reflectance (ATR), which creates spectra equivalent to transmittance.

2.6. Tensile tests

To perform tensile test, two types of bulk specimens were manufactured. Due to their dimensions, standard "dog-bone" tensile specimens would need large seawater containers and longer immersion times to carry out the aging test. Consequently, reduced-scale specimens were manufactured to make the experiment manageable. These methodology was previously produced and validated by other authors [26,34,35]. Standard "dog-bone" specimens were manufactured from 2 mm thick plates by machining (ISO 2818) according to British Standard BS 2782 [36], 150 mm long, 10 mm at its narrowest part. Reduced-scale specimens were manufactured from 1 mm thick plates with the following dimensions: 60 mm length, 10 mm width. Every sample was measured with a caliper before performing tests.

An Instron® universal testing machine model 3367 with a load cell capacity of 30 kN (Norwood, Massachusetts, USA) was used to perform the tensile tests at the rate of 1 mm/min. Prior aging, standard "dog-bone" and reduced-scale specimens were tested at room temperature for validation of the method. After aging, the surface of the reduced-scale specimens was dried with a paper towel, measured with a caliper, and tested at room temperature. The displacements were measured using a Digital Image Correlation (DIC) System [37] and loads were obtained directly from the universal testing machine.

2.6.1. Validation of the reduced-scale specimens

The representative stress vs. strain curves for both standard "dog-bone" and reduced-scale specimens are presented in Fig. 5. The main reason for the observed difference in strain values between the two types of specimens is the volume subjected to stress, because it is greater in the case of "dog-bone".

Mechanical properties are shown in Table 2. In view of the results, as the stiffness and tensile strength present low error values, it can be inferred that the reduced-scale specimens can be used to characterize the Young's modulus and strength of the adhesive.

2.7. Numerical simulation

The porosity of the adhesive was measured by physisorption with an Accelerated Surface Area and Porosimetry System ASAP™ 2020 V4.03 of Micromeritics Instrument Corp. (USA).

The radius of the pore was determined with a JSM-7200F high-resolution scanning electron microscope (SEM) by JEOL Ltd. (Japan). The sample was achieved by fracturing a sheet 1 mm thick in liquid nitrogen and coated with platinum palladium.

3. Results and discussions

3.1. Water uptake behavior

The results of the gravimetric experiments are shown in Fig. 6, in which the percentage (with respect to initial mass of each specimen) of water uptake was determined as a function of time. Considering that the obtained trends are of the asymptotic type, a nonlinear function such as the corresponding to the Fick's law can be a proper candidate to explain the mass water changes. P-splines fittings are included, helping to show the differences of water absorption when load is varied [38].

The effect of time and load over the water uptake can be also studied by fitting Generalized Additive Models (GAM). These semiparametric regression models are an extension of the multivariate linear models, including the addition of smooth effects of predictors in the response. Fig. 7 shows the effects of time and load on the water uptake. Effectively, the effect of time over the water uptake is an asymptotic type: the rate of change is decreasing from a maximum to zero slope in an exponential way. Moreover, the effect of the load is significantly different from zero.

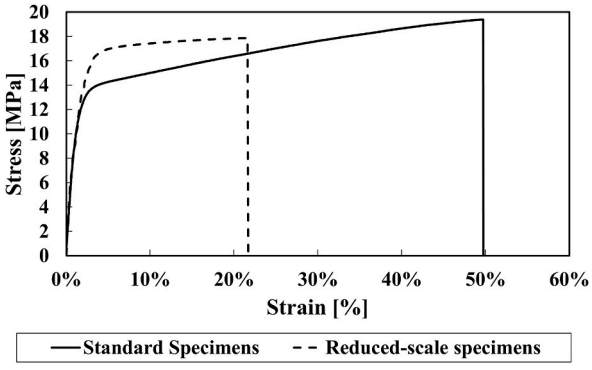

Fig. 5. Validation of the reduced-scale specimens: representative stress vs. strain curves.

Table 2
Mechanical properties of standard "dog-bone" and reduced-scale specimens at room temperature.

Property	Standard "dog-bone" specimens	Reduced-scale specimens	Error
Young's Modulus [GPa]	1.4 ± 0.1	1.3 ± 0.1	6.1%
Tensile Strength [MPa]	19.4 ± 0.1	17.9 ± 0.1	7.8%

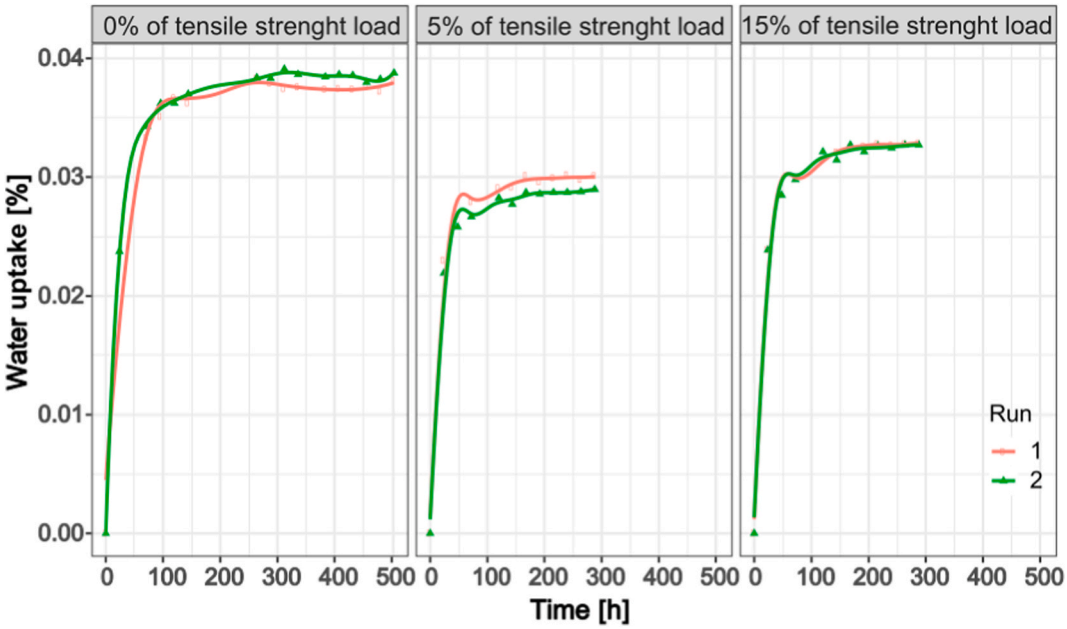

Fig. 6. Water uptake as a function of time and applied load. P-splines regression models have been fitted to real data.

The mass of seawater absorbed by the adhesive is almost totally explained by the effect of time and the magnitude of the applied load ($R^2 = 0.981$). Thus, the water uptake increased in an asymptotic way as a function of time. In addition, when a load is applied, the adhesives tend to absorb less mass of water. The absorbed mass of water is higher when a relatively high load is applied (15% of tensile strength), when compared with the application of a low load (5%). Summarizing, the application of load produces a lower absorption

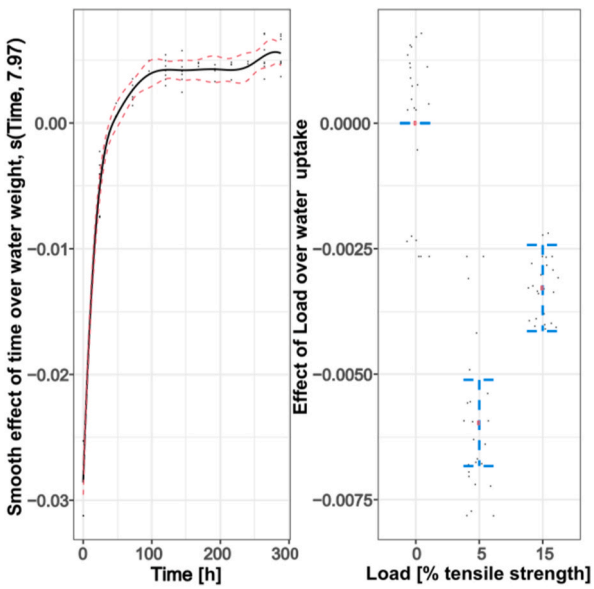

Fig. 7. Effects of time and load on the water uptake estimated by fitting a GAM model based on P-splines.

of water (if compared with no load case), but this mass of absorbed water is increased when the level of load is also increased in the studied range.

A Fick's law of diffusion can be fitted to the experimental results for the three conditions studied. The Fick's law [23] is given by Equation (3).

$$M_t = \left[1 - \frac{8}{\pi^2}\sum_{n=0}^{\infty}\frac{1}{(2n+1)^2}exp\left(\frac{-D(2n+1)^2\pi^2 t}{4h^2}\right)\right]M_\infty \tag{3}$$

where t represents time starting from the immersion and h represents the thickness of the specimen. Therefore, a script developed by the authors was run in Octave free software to determine the best fit of the coefficient of diffusion, D, and infinite water uptake, M_∞, using the least squares method to estimate the model parameters. The values of the parameters estimated, corresponding to each material and each load applied, are given in Table 3.

A comparison of water uptake behavior obtained experimentally, and analytical curves calculated with the Fick Model for the three conditions studied is given in Fig. 8. Standard deviation is indicated for each experimental value as a measure of how dispersed the data is in relation to the mean.

3.2. Numerical simulation of water absorption

Diffusion theory handles two concepts that are different from each other but closely related: on the one hand, the collective movement of particles and, on the other, that of an individual particle [28]. The former is based on Fick's law of diffusion and the second on Darcy's law. Fick's law is the most popular approach to study diffusion. However, in this work Darcy's law was applied for simulation the seawater absorption in the adhesive studied.

To simulate the absorption of seawater in an adhesive sheet, Darcy's law equation (4) combined with the continuity equation (5) are used.

$$\frac{\partial}{\partial t}\left(\varepsilon_p \rho\right) + \nabla \bullet (\rho u) = Q_m \tag{4}$$

$$u = \frac{-k}{\mu}\nabla p \tag{5}$$

where ρ is the density of the fluid (kg/m^3), ε_p is the porosity, Q_m is a mass source term (kg/(m^3·s)) k is the permeability of the porous medium (m^2); μ is the dynamic viscosity of the fluid (Pa·s) and p is the capillary pressure (N/m^2). Porosity is defined as the fraction of the control volume that is occupied by pores. The material parameters are presented in Table 4.

In addition, in a capillary model – in which the medium is assumed to be a bundle of capillary tubes, see Fig. 9 permeability can be obtained by equation (6) [39]:

$$k = \frac{1}{8}\varepsilon_p R_P^2 \tag{6}$$

where R_p is the radius of the pore, that was determined with high-resolution scanning electron microscope (SEM) as seen in Fig. 10.

The radius of the pore was determined from Fig. 10.

Capillary pressure in tubes can be calculated with the following equation (7) [40]:

$$P_c = \frac{2\sigma\, cos\,\theta}{R_p} \tag{7}$$

where P_c is the capillary pressure (N/m^2) and θ and σ are the contact angle (degrees) and surface tension (N/m) [41], respectively. In this case the contact angle is cero.

The whole set of equations is solved in Comsol Multiphysics for given conditions. In Fig. 11 it is appreciated the absorption of water along the time by the adhesive at 0% load, reaching saturation at 450 h. Simulation shows coherence with the experimental data and analytical model according Fick's Law presented in Fig. 8.

Fig. 12 shows a comparative between numerical simulation according to Darcy's Law, analytical data obtained following Fick's

Table 3
Seawater uptake properties at different applied loads.

Load	D (m^2/s)	M_∞ (%)
0%	7.55×10^{-13}	3.78
5%	11.15×10^{-13}	2.93
15%	9.95×10^{-13}	3.27

It is observed that when a load is applied, the value of the diffusion coefficient increases (the absorption rate is higher), but the amount of water absorbed is lower (saturation is reached earlier).

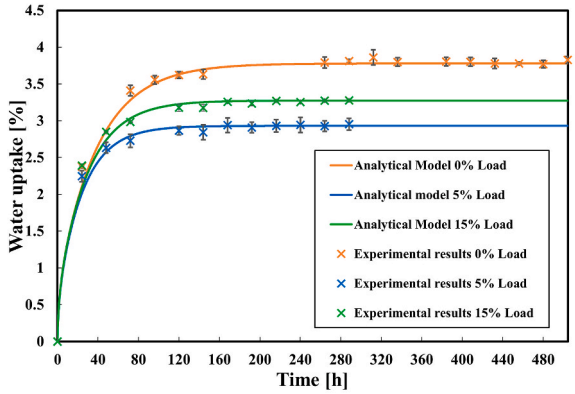

Fig. 8. Comparison between experimental results and Fickian water uptake behavior for constant loads of 0%, 5% and 15% of the tensile strength.

Table 4
Material properties.

Property	Value
Density water (kg•m^{-3})	1015
Surface tension (N•m^{-1})	0.0688
Viscosity of water (Pa•s)	5.5 E^{-4}
Porosity	0.1
Porous radius (nm)	12.5

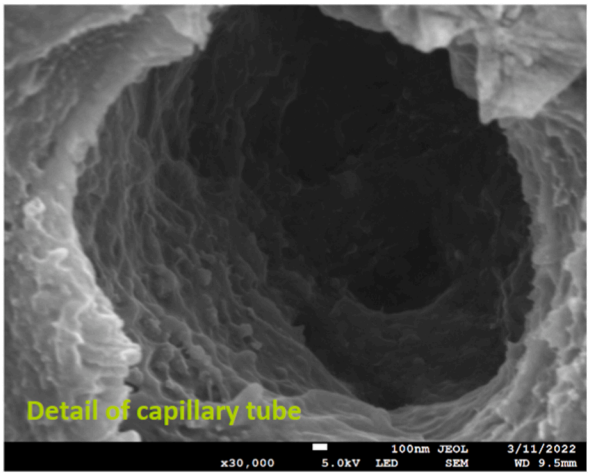

Fig. 9. Image of the adhesive taken with a scanning electron microscope (SEM) (Observation magnification: ×30.000, accelerating voltage: 5.0 kV; detector: LED; resolution: 100 nm; working distance (WD): 9.5 mm): inside detail of a pore in which the shape of a tube is appreciated.

Law and experimental results.

Summarizing, it was found a good correlation between the experimental data and numerical results according to both Darcy's and Fick's Laws models.

3.3. Thermal analysis

The results from DSC analysis are presented in Fig. 13. There are disturbances corresponding to the glass transition temperature (T_g), which take place over a temperature range. To determine a single number for the T_g, the extrapolated onset temperature (T_f), the mid-point temperature (T_m), the inflection temperature (T_i), and the extrapolated end temperature (T_e) were determined automatically by the computer control software. According to ASTM E1356-08 [42], the mid-point (T_m), computed as the mean between T_f and T_e was chosen as T_g value, since is the most commonly used, being constructed closer to the middle of the temperature range over with the

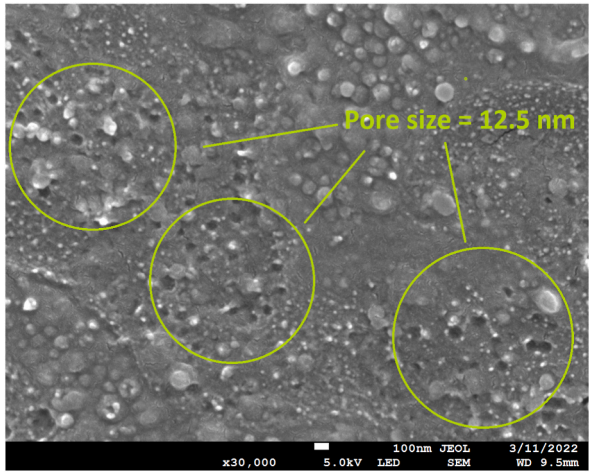

Fig. 10. Image of the adhesive taken with a scanning electron microscope (SEM) (Observation magnification: ×30.000; accelerating voltage: 5.0 kV; detector: LED; resolution: 100 nm; working Distance (WD): 9.5 mm).

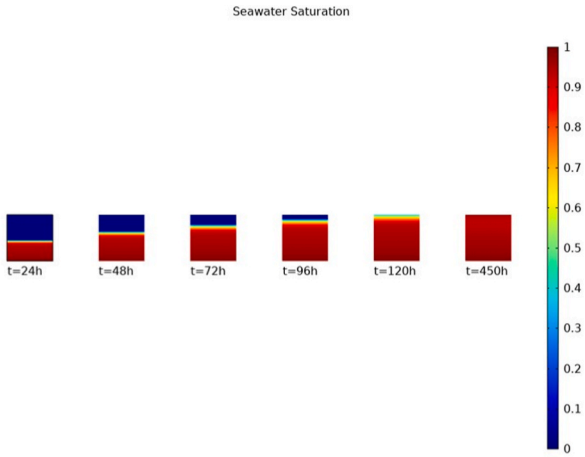

Fig. 11. Amount of water absorbed during the aging process (0% Load condition).

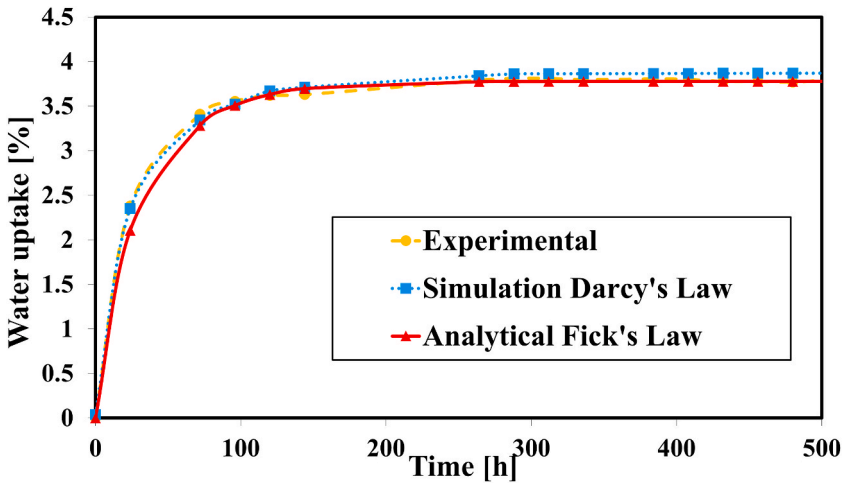

Fig. 12. Comparison of water uptake percentage on time for aging at 0% Load condition.

glass transition occurs. The aging process was carried out at 48 °C, which is 78.5 °C below the Glass Transition Temperature (T_g) of the adhesive under analysis. So, in the aged specimens the T_g values are 82.4 °C, 81.9 °C, 78.3 °C for respectively 0%, 5% and 15% load condition, and 126.5 °C for the unaged (dried) one: There is a considerable reduction in the T_g after aging, as the absorbed water alters adhesive properties in a reversible manner producing plasticization [43]. There is a trend as with the increase of load, the T_g decreases. It is suggested that with application of higher loads, this drop of T_g will be more pronounced. Moreover, for temperatures above 160 °C it is observed the melting temperature of the adhesives. Also, endothermic peaks corresponding to enthalpic relaxation are observed in the aged samples, which are superimposed on the glass transition temperature range. By contrast, this is not presented in the dried specimen. The presence or absence of enthalpic relaxation depends on the time the specimens spend below the T_g. Temperatures near to T_g facilitate the presence of enthalpic relaxation. This can explain that samples aged at 48 °C present enthalpic relaxation and the unaged one does not [44].

3.4. Chemical structure analysis

FTIR Spectroscopy was carried out to analyze the chemical degradation produced during the aging process. Transmittance spectra is showed in Fig. 14, where tests have been made before immersion in seawater and after aging with constant loads of 0%, 5% and 15% of the tensile strength.

The peak around 3400 cm^{-1}, correspondent to the presence of the hydroxyl group (OH^-) is the consequence of the absorption of water during the immersion time, which could be explained when the free space of the adhesive is occupied by water molecules or due to chemical interactions between the absorbed water and the adhesive. The latter can be explained through the creation of chemical bonds with water as bound water, forming single or multiple hydrogen bonds with the polymer chain of the adhesive or either due to hydrolysis of the ester group (C═O) of MMA obtaining alcohol and carboxylic acid (-COOH). Polymers have been known to undergo this hydrolysis when immersed in acid conditions at high temperatures, which did not happen in this case, as pH of seawater is around 8 and the experiment was not carried out at high temperature, but at 48 °C [20,45,46]. The explanation of hydrogen bonding is also discarded because it reduces the free volume of the adhesive, increasing the T_g [43], and this is contradictory with the remarkable decreasing values observed in the DSC. In addition, no differences are observed in the rest of the bands of the spectra, there is no change in the chemical composition of the adhesive for the conditions studied. So, absorption of seawater is produced through the occupation of the free space into the polymeric chain of the adhesive.

There are different values of transmittance for the different conditions tested. Transmittance decreases as the concentration of the analyte (OH^-) increases, so the presence of water is maximum for 15% load. Sample with 5% load might be expected to present more water absorption than 0% one, but its transmittance is 7% lower. This difference can be considered not significant, as it is referred to a low range.

3.5. Mechanical properties

Representative stress-strain curves for unaged and aged specimens with three different loads analyzed are presented in Fig. 15.

Results shown in Table 5 that there is at first a slight decrease in tensile strength after aging and an improvement as the load is higher. The stiffness decreases initially, as said, but increases as the applied load is greater. Previous studies have found that water initially plasticizes the adhesive, causing a fall in modulus, but improving or without changing its strength [15,21,47]. Therefore, in the range studied, the application of loads during immersion in seawater improves the strength and increases the stiffness of the adhesive.

The results for tensile strength as a function of water uptake for 0%, 5%, and 15% constant loads are presented in Fig. 16. There is a slight linear inverse relationship between the tensile strength and the water uptake. When the water is increasing, the tensile strength tends to decay.

The results for Young's modulus as a function of water uptake for 0%, 5% and 15% load are given in Fig. 17.

It can be deduced that there is not a clear trend in any of the loads analyzed for the evolution of Young's modulus values as a function of the water uptake.

3.5.1. Relation between load and Poisson's coefficient

Poisson ratio was defined originally as a "constant value for elastic, isotropic materials, linking the transverse to the longitudinal deformations upon uniaxial loading". For materials with viscoelastic properties, such as adhesives, which are time and temperature dependent, the Poisson ratio varies with time and temperature and can be considered as not constant. Poisson's ratios were determined for each condition studied, measuring the longitudinal and transversal directions during tensile tests with a Digital Image Correlation (DIC) System and GOM Correlate software, as seen in Fig. 18.

Range between 0.2 and 0.5 is expected for macroscopically homogeneous materials as this adhesive [48]. Besides, the values obtained closed to 0.3 are the expected ones for temperatures below the glass transition temperature (T_g) [31].

Poisson's coefficients are very similar in Fig. 19 for unaged of standard (dog-bone) and reduced specimens. The ratio decreases with the immersion in seawater and increases as the load conditions are applied.

Since temperature is not in this case a determining factor in the change in Poisson's ratio, the applied constant loads must be considered. In addition, diffusion is an omnipresent phenomenon matched to porous media, and adhesives can be considered virtually as porous [28]. Consequently, it is suggested to also consider the dependence relationship between Poisson's ratio and porosity in porous materials such as the adhesives studied here presented by Kovacik, who proposed a model to describe this relationship limited

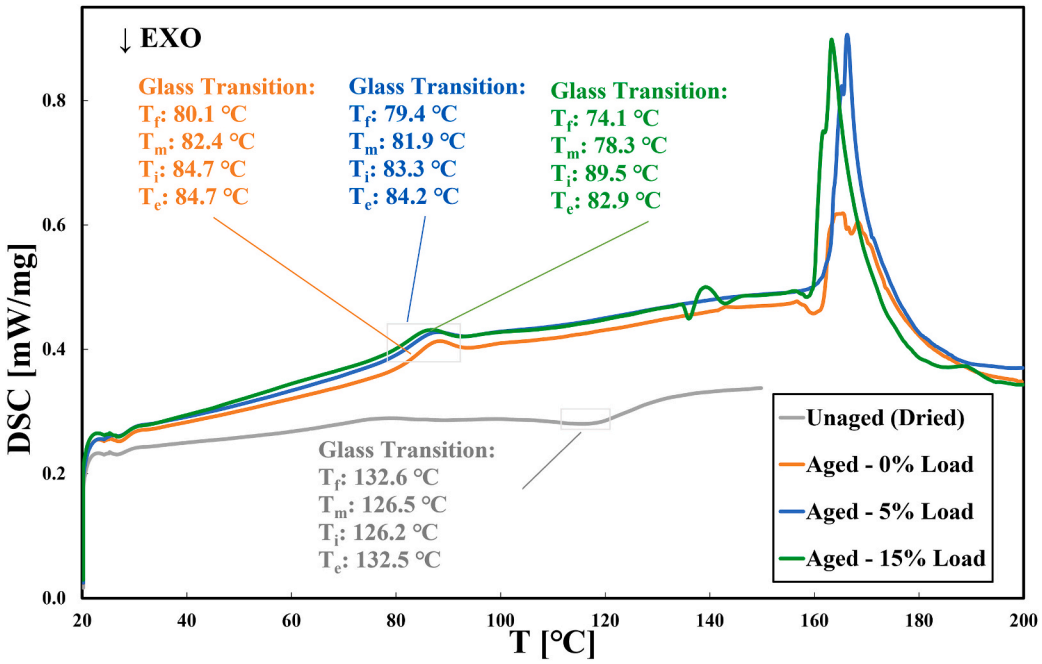

Fig. 13. Representative DSC curves for Methyl Methacrylate-based adhesive at different conditions.

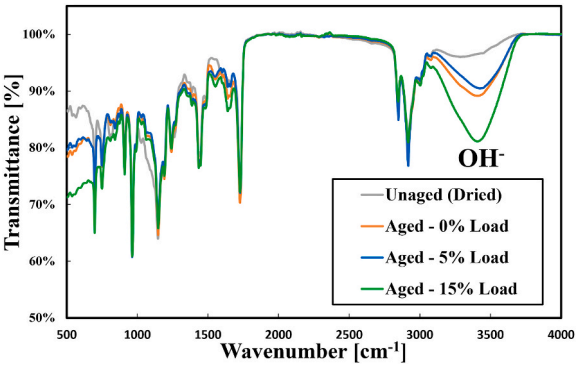

Fig. 14. FTIR results for Methyl Methacrylate-based adhesive unaged (dried) and after aging in seawater with constant loads of 0%, 5% and 15% of the tensile strength (20.7 MPa). Chemical changes are found in region 3500–3000 related to OH^-.

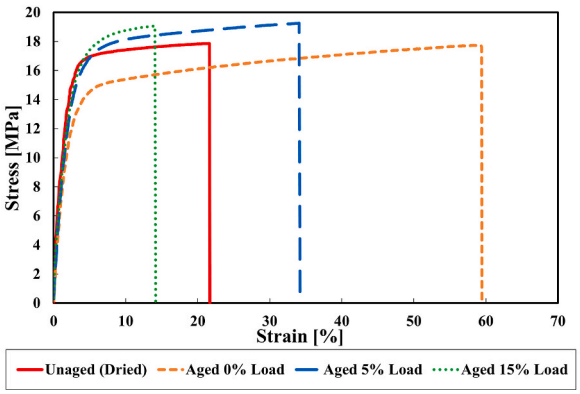

Fig. 15. Tensile tests of dried and aged specimens at different loads applied: representative stress vs. strain curves.

Table 5
Tensile tests results before aging and after immersion with different constant loads applied.

Property	Unaged	Aged 0% Load	Aged 5% Load	Aged 15% Load
Young's Modulus (GPa)	1.3 ± 0.1	0.9 ± 0.1	1.0 ± 0.1	1.8 ± 0.1
Tensile strength (MPa)	17.9 ± 0.1	17.7 ± 0.1	19.3 ± 0.1	19.1 ± 0.1

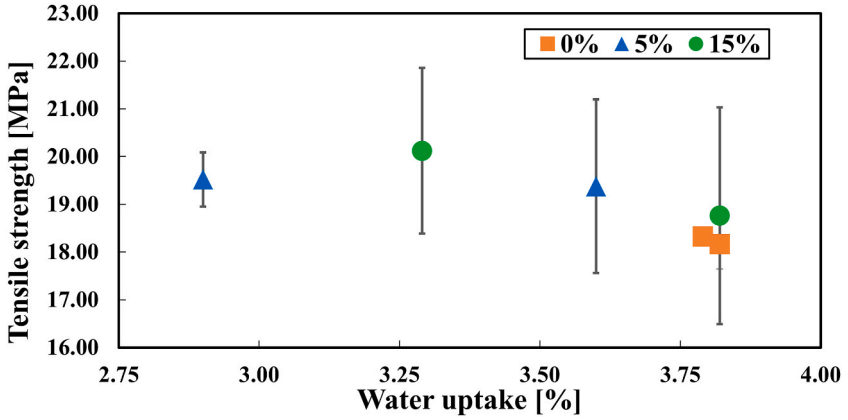

Fig. 16. Tensile strength of adhesive specimens aged with different loads 0%, 5%, 15% as a function of water uptake.

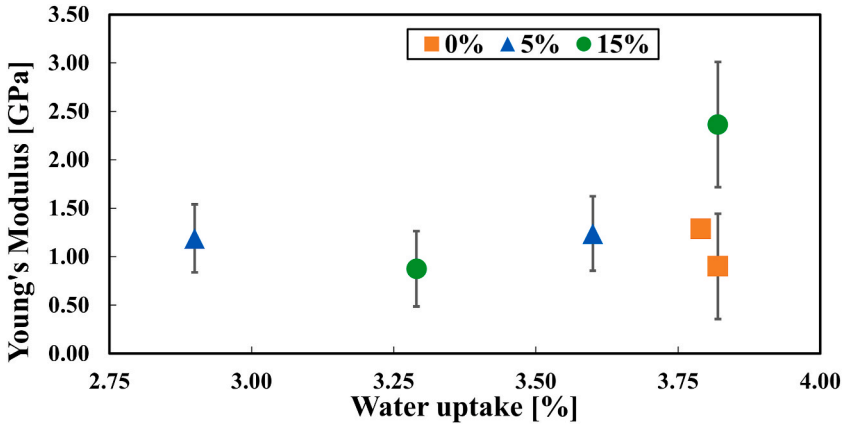

Fig. 17. Stiffness of adhesive specimens aged with different loads 0%, 5%, 15% as a function of water uptake.

to isotropic and homogeneous materials [49].

4. Conclusions

The experimental results are fitted to Fick's law of diffusion for the load conditions studied, concluding the seawater diffusion behavior is Fickian. The diffusion coefficients determined reveal that velocity of absorption increases significatively with load.

The relationship between the effect of time, load applied, and the amount of water absorbed, is demonstrated by fitting Generalized Additive Models, concluding that when a load is applied, the adhesive tends to absorb less mass of water. However, as the level of load increases, the amount of water absorbed is larger.

A novel approach FEM water uptake simulation, for no load condition, was carried out applying Darcy's law, finding a good correlation with experimental data and numerical results according to Fick's law model. It is possible, therefore, to predict the amount of water absorbed by the adhesive at each instant of time.

There is a considerable decrease in the glass transition temperature after aging. Furthermore, as the applied load increases, this decline is more pronounced.

FTIR results show that the chemical composition of the adhesive does not change, and that the water absorption in the polymeric chain of the adhesive is higher as the applied load increases.

Immersion in seawater until full saturation produces initially plasticization, producing a drop in the modulus value without

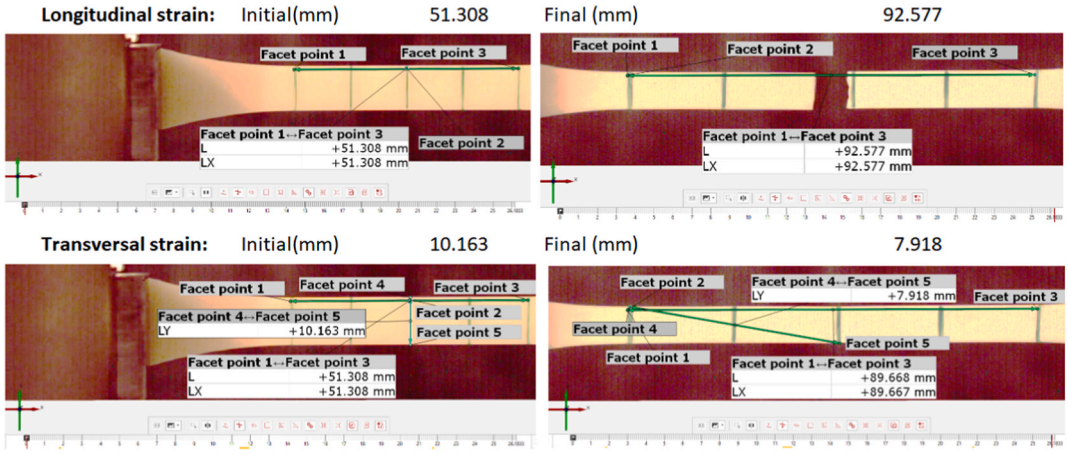

Fig. 18. Measurement of the longitudinal and transversal directions during tensile tests with a Digital Image Correlation (DIC) System and GOM Correlate software.

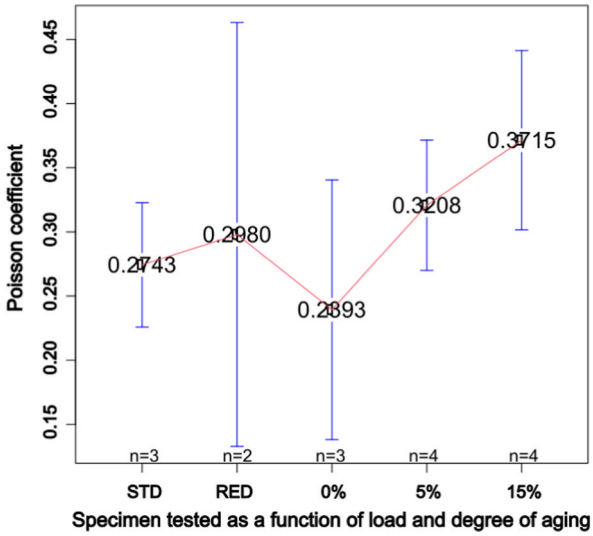

Fig. 19. Poisson's coefficient for every specimen tested. Mean values and corresponding 95% confidence intervals.

changes in strength. The application of loads improves the strength and increases the stiffness of the adhesive.

The results support the possibility of a relationship between Poisson's ratio and water absorption due to load application.

Immersion in seawater and application of loads enhance the mechanical properties of the adhesive, promoting its use in shipbuilding. However, the influence of loads applied in the drop of glass transition temperature is suggested to be considered in future works.

Author contribution statement

Francisco Javier Rodríguez Dopico: Conceived and designed the experiments; Performed the experiments; Analyzed and interpreted the data; Contributed reagents, materials, analysis tools or data; Wrote the paper.

Ricardo J.C. Carbas: Conceived and designed the experiments; Performed the experiments; Analyzed and interpreted the data; Contributed reagents, materials, analysis tools or data.

Catarina S. P. Borges: Performed the experiments.

Javier Tarrío-Saavedra: Analyzed and interpreted the data; Contributed reagents, materials, analysis tools or data.

Lucas Filipe Martins da Silva: Conceived and designed the experiments; Contributed reagents, materials, analysis tools or data.

Ana Álvarez García: Conceived and designed the experiments; Analyzed and interpreted the data; Contributed reagents, materials, analysis tools or data; Wrote the paper.

Funding statement

This research did not receive any specific grant from funding agencies in the public, commercial, or not-for-profit sectors.

Data availability statement

Data will be made available on request.

Declaration of interest's statement

The authors declare no competing interests.

Acknowledgements

The research of Javier Tarrío Saavedra has been supported by the Ministerio de Ciencia e Innovación grant PID2020-113578RB-100, the Xunta de Galicia (Grupos de Referencia Competitiva ED431C-2020-14), and by the CITIC, also funded by the Xunta de Galicia through the collaboration agreement between the Consellería de Cultura, Educación, Formación Profesional e Universidades and the Galician universities for the reinforcement of the research centers of the Galician University System (CIGUS).

References

[1] C.-H. Lai, C.-C. Chou, H.-C. Chuang, G.-J. Lin, C.-H. Pan, W.-L. Chen, Receptor for advanced glycation end products in relation to exposure to metal fumes and polycyclic aromatic hydrocarbon in shipyard welders, Ecotoxicol. Environ. Saf. 202 (2020) 110920, https://doi.org/10.1016/j.ecoenv.2020.110920.
[2] C.-H. Lai, et al., Chronic exposure to metal fume PM2.5 on inflammation and stress hormone cortisol in shipyard workers: a repeat measurement study, Ecotoxicol. Environ. Saf. 215 (2021) 112144, https://doi.org/10.1016/j.ecoenv.2021.112144.
[3] D.-H. Koh, S.-W. Lee, B.-J. Ye, J.-I. Kim, Grouping schemes of welding fume exposure in shipyard welders, J. Occup. Environ. Hyg. 15 (5) (May 2018) 413–421, https://doi.org/10.1080/15459624.2018.1447115.
[4] M. Mejri, J.-Y. Cognard, Time-variant assessment for adhesively bonded assemblies with non-linear behaviour in naval applications, Ships Offshore Struct. 4 (3) (Oct. 2009) 275–286, https://doi.org/10.1080/17445300903149020.
[5] M. Perčić, I. Ančić, N. Vladimir, Life-cycle cost assessments of different power system configurations to reduce the carbon footprint in the Croatian short-sea shipping sector, Renew. Sustain. Energy Rev. 131 (2020) 110028, https://doi.org/10.1016/j.rser.2020.110028.
[6] N. Vladimir, I. Ančić, A. Šestan, Effect of ship size on EEDI requirements for large container ships, J. Mar. Sci. Technol. 23 (1) (2018) 42–51, https://doi.org/10.1007/s00773-017-0453-y.
[7] 'Third IMO GHG Study 2014'. https://www.imo.org/en/OurWork/Environment/Pages/Greenhouse-Gas-Studies-2014.aspx, 2022.
[8] J.R. Weitzenböck, Adhesives in Marine Engineering, first ed., Woodhead Publishing, 2012. Accessed: Nov. 14, 2021. [Online]. Available: https://www.elsevier.com/books/adhesives-in-marine-engineering/weitzenbock/978-1-84569-452-4.
[9] B. Sánchez Silva, Estudio de adhesivos para la construcción naval mediante análisis térmico y reológico, Universidade da Coruña, 2021. Accessed: Nov. 05, 2022. [Online]. Available: https://ruc.udc.es/dspace/handle/2183/28746.
[10] B. Sánchez-Silva, A. Díaz-Díaz, J. Tarrío-Saavedra, J. López-Beceiro, C.A. Gracia-Fernández, R. Artiaga, Thermal and rheological comparison of adhesives, J. Therm. Anal. Calorim. 138 (5) (2019) 3357–3366, https://doi.org/10.1007/s10973-019-08882-6.
[11] J. Cantrill, A. Kapadia, D. Pugh, Lessons learnt from designing and producing adhesively bonded prototyping structures in a shipyard, Proc. Inst. Mech. Eng. Part M J. Eng. Marit. Environ. 218 (4) (Dec. 2004) 267–272, https://doi.org/10.1177/147509020421800406.
[12] Bonding of lightweight materials for cost effective production of high speed craft and passenger ships (BONDSHIP) | BONDSHIP Project | Results | FP5 | CORDIS | European Commission. https://cordis.europa.eu/project/id/G3RD-CT-2000-00101/results.
[13] D. Mathijsen, Now is the time to make the change from metal to composites in naval shipbuilding, Reinforc Plast 60 (5) (Sep. 2016) 289–293, https://doi.org/10.1016/j.repl.2016.08.003.
[14] D.R. Speth, Y.P. Yang, G.W. Ritter, Qualification of adhesives for marine composite-to-steel applications, Int. J. Adhesion Adhes. 30 (2) (Mar. 2010) 55–62, https://doi.org/10.1016/j.ijadhadh.2009.08.004.
[15] E. Lertora, C. Gambaro, C. Mandolfino, M. Pedemonte, Environmental effects on methacrylate adhesive, Weld. Int. 28 (5) (May 2014) 372–379, https://doi.org/10.1080/09507116.2012.753261.
[16] M. Ortega-Iguña, A. Akhavan-Safar, R.C.J. Carbas, J.M. Sánchez-Amaya, M. Chludzinski, L.F.M. da Silva, Use of seawater to improve the static strength and fatigue life of bonded coated steel joints, Polym. Degrad. Stabil. 206 (2022) 110169, https://doi.org/10.1016/j.polymdegradstab.2022.110169.
[17] N. Arnaud, R. Créac'hcadec, J.Y. Cognard, P. Davies, P.Y. Le Gac, Analysis of the moisture effect on the mechanical behaviour of an adhesively bonded joint under proportional multi-axial loads, J. Adhes. Sci. Technol. 29 (21) (2015) 2355–2380, https://doi.org/10.1080/01694243.2015.1067018.
[18] H. Hayashibara, T. Iwata, T. Ando, C. Murakami, E. Mori, I. Kobayashi, Degradation of structural adhesive bonding joints on ship exposure decks, J. Mar. Sci. Technol. 25 (2) (2020) 510–519, https://doi.org/10.1007/s00773-019-00657-w.
[19] A.W. Momber, L. Fröck, T. Marquardt, Effects of accelerated ageing on the mechanical properties of adhesive joints between stainless steel and polymeric top coat materials for marine applications, Int. J. Adhesion Adhes. 103 (2020) 102699, https://doi.org/10.1016/j.ijadhadh.2020.102699.
[20] C. Alia, M.V. Biezma, P. Pinilla, J.M. Arenas, J.C. Suárez, Degradation in seawater of structural adhesives for hybrid fibre-metal laminated materials, Adv. Mater. Sci. Eng. 2013 (2013) e869075, https://doi.org/10.1155/2013/869075.
[21] P. Davies, Marine industry, in: L.F.M. da Silva, A. Öchsner, R.D. Adams (Eds.), Handbook of Adhesion Technology, Springer International Publishing, Cham, 2018, pp. 1391–1417, https://doi.org/10.1007/978-3-319-55411-2_48.
[22] R. Carbas, L.F.M. Silva, E. Marques, A. Lopes, Effect of post-cure on the glass transition temperature and mechanical properties of epoxy adhesives, J. Adhes. Sci. Technol. 27 (2013) 2542–2557.
[23] A. Fick, On liquid diffusion, J. Membr. Sci. 100 (1) (1995) 33–38, https://doi.org/10.1016/0376-7388(94)00230-V.
[24] K. Houjou, K. Shimamoto, H. Akiyama, C. Sato, Effect of cyclic moisture absorption/desorption on the strength of epoxy adhesive joints and moisture diffusion coefficient, J. Adhes. 0 (0) (May 2021) 1–17, https://doi.org/10.1080/00218464.2021.1926242.
[25] J. Brettle, D.M. Brewis, J. Comyn, B.C. Cope, M.T. Goosey, R.D. Hurditch, The interaction of water with an epoxide adhesive based on the diglycidylether of bisphenol-A and triethylene tetramine, Int. J. Adhesion Adhes. 3 (4) (Oct. 1983) 189–192, https://doi.org/10.1016/0143-7496(83)90092-1.
[26] C.S.P. Borges, et al., Effect of water ingress on the mechanical and chemical properties of polybutylene terephthalate reinforced with glass fibers, Materials 14 (5) (Jan. 2021), https://doi.org/10.3390/ma14051261. Art. no. 5.
[27] Y. Chen, M. Chen, X. Tong, S. Wang, X. Kang, Molecular insights into the interactions between chloride liquids and CSH nanopore surfaces under electric field-induced transport, J. Mol. Liq. 364 (2022) 119942, https://doi.org/10.1016/j.molliq.2022.119942.

[28] D.M. Tartakovsky, M. Dentz, Diffusion in porous media: phenomena and mechanisms, Transport Porous Media 130 (1) (Oct. 2019) 105–127, https://doi.org/10.1007/s11242-019-01262-6.
[29] V.M. Starov, A.G.F. Stapley, V.G. Zhdanov, Effective properties of porous and composite materials, J. Adhes. 80 (10–11) (2004) 971–1002, https://doi.org/10.1080/00218460490509309.
[30] AFNOR, 'NF T 76-142', AFNOR Editions, Jul. 2021. Accessed: Feb. 20, 2022. [Online]. Available: https://m.boutique.afnor.org/en-gb/standard/nf-t-76142/structural-adhesives-preparation-method-of-structural-adhesive-plates-for-c/fa194492/238796.
[31] L.F.M. da Silva, R.J.C. Carbas, M.D. Banea, Failure strength tests, in: L.F.M. da Silva, A. Öchsner, R.D. Adams (Eds.), Handbook of Adhesion Technology, Springer International Publishing, Cham, 2018, pp. 489–521, https://doi.org/10.1007/978-3-319-55411-2_19.
[32] L.F.M. da Silva, R.D. Adams, M. Gibbs, Manufacture of adhesive joints and bulk specimens with high-temperature adhesives, Int. J. Adhesion Adhes. 24 (1) (2004) 69–83, https://doi.org/10.1016/S0143-7496(03)00101-5.
[33] A. Khabaz-Aghdam, B. Behjat, L.F.M. da Silva, E.A.S. Marques, A new theoretical creep model of an epoxy-graphene composite based on experimental investigation: effect of graphene content, J. Compos. Mater. 54 (18) (2020) 2461–2472, https://doi.org/10.1177/0021998319895806.
[34] M. Costa, et al., Effect of the size reduction on the bulk tensile and double cantilever beam specimens used in cohesive zone models, Proc. Inst. Mech. Eng. Part J. Mater. Des. Appl. 230 (5) (Oct. 2016) 968–982, https://doi.org/10.1177/1464420715610248.
[35] G. Viana, M. Costa, M.D. Banea, L.F.M. da Silva, Behaviour of environmentally degraded epoxy adhesives as a function of temperature, J. Adhes. 93 (1–2) (Jan. 2017) 95–112, https://doi.org/10.1080/00218464.2016.1179118.
[36] BSI, 'BS 2782, Methods of Testing Plastic', BSI, 2011. Accessed: Nov. 13, 2021. [Online]. Available: https://shop.bsigroup.com/products/methods-of-testing-plastic-introduction/preview.
[37] M.A. Sutton, J.J. Orteu, H. Schreier, Image Correlation for Shape, Motion and Deformation Measurements: Basic Concepts,Theory and Applications, Springer Science & Business Media, 2009.
[38] S.N. Wood, Generalized Additive Models: an Introduction with R, Chapman & Hall, Boca Raton [etc., 2006.
[39] F.A.L. Dullien, Porous Media: Fluid Transport and Pore Structure, second ed., Academic Press, San Diego, 1992.
[40] A. Zankoor, M. Khishvand, A. Mohamed, R. Wang, M. Piri, In-situ capillary pressure and wettability in natural porous media: multi-scale experimentation and automated characterization using X-ray images, J. Colloid Interface Sci. 603 (Dec. 2021) 356–369, https://doi.org/10.1016/j.jcis.2021.06.052.
[41] K.G. Nayar, D. Panchanathan, G.H. McKinley, J.H. Lienhard, Surface tension of seawater, J. Phys. Chem. Ref. Data 43 (4) (2014) 43103, https://doi.org/10.1063/1.4899037.
[42] ASTM International, Standard Test Method for Assignment of the Glass Transition Temperatures by Differential Scanning Calorimetry. https://www.astm.org/e1356-08r14.html.
[43] Y. Zhang, R.D. Adams, L.F.M. da Silva, Absorption and glass transition temperature of adhesives exposed to water and toluene, Int. J. Adhesion Adhes. 50 (Apr. 2014) 85–92, https://doi.org/10.1016/j.ijadhadh.2014.01.022.
[44] J.J.L. Beceiro, Modelización de la transición vítrea con relajación entálpica a partir de datos térmicos, Universidade da Coruña, 2011.
[45] W.N. Ayre, S.P. Denyer, S.L. Evans, Ageing and moisture uptake in polymethyl methacrylate (PMMA) bone cements, J. Mech. Behav. Biomed. Mater. 32 (Apr. 2014) 76–88, https://doi.org/10.1016/j.jmbbm.2013.12.010.
[46] J.A. da Costa, A. Akhavan-Safar, E.A.S. Marques, R.J.C. Carbas, L.F.M. da Silva, Cyclic ageing of adhesive materials, J. Adhes. 0 (0) (Mar. 2021) 1–17, https://doi.org/10.1080/00218464.2021.1895772.
[47] M.R. Bowditch, The durability of adhesive joints in the presence of water, Int. J. Adhesion Adhes. 16 (2) (May 1996) 73–79, https://doi.org/10.1016/0143-7496(96)00001-2.
[48] M. Angelidi, A.P. Vassilopoulos, T. Keller, Displacement rate and structural effects on Poisson ratio of a ductile structural adhesive in tension and compression, Int. J. Adhesion Adhes. 78 (Oct. 2017) 13–22, https://doi.org/10.1016/j.ijadhadh.2017.06.008.
[49] J. Kováčik, Correlation between Poisson's ratio and porosity in porous materials, J. Mater. Sci. 41 (4) (2006) 1247–1249, https://doi.org/10.1007/s10853-005-4237-0.